Available online at www.sciencedirect.com
ScienceDirect
Trans. Nonferrous Met. Soc. China 35(2025) 2217−2226
Transactions of Nonferrous Metals Society of China
www.tnmsc.cn

Effect of Ag micro-alloying on elevated-temperature creep resistance of Mg−Gd−Y−Zr extrusion bars

Dong-dong ZHANG[1], Chu-ming LIU[2], Ying-jie HUANG[1],
Yong-hao GAO[1], Shu-nong JIANG[1], Ying-chun WAN[3], Zhi-yong CHEN[1]

1. School of Materials Science and Engineering, Central South University, Changsha 410083, China;
2. Hunan Meiyu Technology Co. Ltd., Yueyang 414000, China;
3. Research Institute of Light Alloy, Central South University, Changsha 410083, China

Received 21 November 2023; accepted 13 July 2024

Abstract: The effects of trace Ag on the tensile strength and creep resistance of Mg−7.5Gd−1.5Y− 0.4Zr (wt.%) extrusion bars were investigated at temperatures of 175−275 °C, via tensile tests and creep tests, electron back-scatter diffraction, and transmission electron microscopy. Adding trace Ag improves the tensile strength and creep resistance of Mg−Gd−Y−Zr alloys at elevated temperatures. During the creep process, precipitate-free zones (PFZs) are formed near grain boundaries and perpendicular to the loading direction, while chain-like β'-Mg_7RE precipitates are distributed in a special direction ($[10\bar{1}0]$) in grain interior. After adding Ag element, the creep resistance of the Mg−Gd−Y−Zr−Ag is improved due to the suppression of dislocation movement by the synergistic effect of narrower PFZs, finer β'-Mg_7RE precipitates in the grain interior and more stable β-Mg_5RE phase located on the grain boundaries.
Key words: trace Ag; creep resistance; precipitate-free zones; extrusion; Mg−Gd−Y−Zr alloy

1 Introduction

Due to the low density and high specific strength, Mg alloys have aroused increasing interest from researchers in the aerospace and transportation industries [1−3]. Despite these merits, the large-scale application of Mg alloys is limited by poor creep resistance when the operating temperature exceeds 200 °C [4,5]. To meet the various demands in automotive, nuclear reactors, and oil exploration, alloying is an effective method for enhancing the creep resistance of Mg alloys.

Alloying elements improve creep resistance by inducing the formation of solute atom segregation/clusters [6,7], thermally stable second phase at grain boundaries [8,9] or thermostable precipitates in the Mg matrix [10,11]. Among Mg alloys with various alloying elements, Mg alloys containing rare earth elements are considered to have the potential to satisfy the serious conditions of high-temperature structural parts in the future [10,12]. For example, Gd and Y have high solid solubility limits at eutectic temperatures, and are able to enhance the creep resistance of Mg alloys by the solid solution strengthening or the precipitation strengthening [13,14].

Moreover, the strengthening effects from solute atoms or precipitates can be further improved by adding micro-alloying elements to Mg−Gd series alloys. For example, Nd promotes the formation of β'-Mg_7RE precipitates or induces a new $Mg_{41}Nd_5$ phase, which contributes to maintaining the excellent creep resistance of Mg−10Gd−3Y−0.5Zr

Corresponding author: Chu-ming LIU, Tel: +86-13974870878, Email: cmliu@csu.edu.cn;
Yong-hao GAO, Tel: +86-18874102281, Email: gaoyonghao_009@163.com
https://doi.org/10.1016/S1003-6326(25)66810-5

(wt.%) alloys at elevated temperatures [15]. Similarly, adding Ag (above 1.5 wt.%) induces the formation of the $Mg_{16}Gd_2YAg$ phase and improves the tensile properties and creep resistance of Mg−Gd series alloys [16,17].

In contrast, trace Ag can improve the strength of Mg−Gd series alloys by inducing solute segregation at grain boundaries or accelerating the precipitation of smaller β'-Mg_7RE phase rather than the formation of $Mg_{16}Gd_2YAg$ phase [4,18]. That is, it is still unclear what roles does trace Ag play in the creep process without the $Mg_{16}Gd_2YAg$ phase. Thus, in this study, Mg−Gd−Y−Zr alloys containing Ag are designed, and used to elucidate how Ag improves the heat resistance of Mg−Gd−Y−Zr alloys, which will provide important insight into developing heat-resistant Mg wrought alloys.

2 Experimental

After melting pure Mg, Mg−30Gd, Mg−30Y, Mg−30Zr, and pure Ag at 750 °C, the 0Ag (Mg−7.89Gd−1.43Y−0.45Zr, wt.%) and 0.5Ag (Mg−7.50Gd−1.53Y−0.37Zr−0.45Ag, wt.%) alloys were cast, and then homogenized at 520 °C for 24 h. Extrusion bars with a diameter of about 18 mm were fabricated at an extrusion temperature of 470 °C and an extrusion ratio of 25 followed by air cooling. The ram speed was about 2 mm/s.

Along the extrusion direction (ED), the tensile strength and tensile creep properties of the 0Ag and 0.5Ag extrusion bars were tested at elevated temperatures. The diameter and gauge length of the samples for tensile tests and tensile creep tests were 5 mm and 30 mm, respectively. Using an Instron 3369 testing machine, the ultimate tensile strength (UTS), tensile yield strength (TYS, offset of 0.2%), and elongation to failure (EL) were obtained at 200 °C and 250 °C. Before loading, samples should be held at a set temperature for at least 10 min in the tensile test. Aided by the RWS50 creep testing machine, when the sample was held at the test temperature for 1 h, conventional tensile creep tests were performed at 175−275 °C and under a constant load of 100 MPa.

The observation planes of all the samples for scanning electron microscopy (SEM) with backscattered electron (BSE) and electron back-scatter diffraction (EBSD) were parallel to the ED. These samples were mechanically ground and then electro-polished in a solution of 4 vol.% perchloric acid and 96 vol.% ethyl alcohol. BSE-SEM images were acquired on a Tescan Mira 3 with an accelerating voltage of 20 kV and a working distance of 10.80 mm. The EBSD data were acquired on a Helios Nanolab 600i with an accelerating voltage of 20 kV and a step size of 5 μm. At an accelerating voltage of 200 kV, transmission electron microscopy (TEM) images and high-angle annular dark-field (HAADF) scanning transmission electron microscopy (STEM) images were acquired, aided by a Talos F200X. The incident electron beams of the TEM image and HAADF-STEM images were parallel to the $[10\bar{1}0]$ and [0001] axes, respectively. The detailed TEM foil preparation process was described in our previous work [19,20].

3 Results

3.1 Initial microstructure

Figure 1 presents the microstructure of the extruded Mg alloys. Under the above extrusion parameters, the 0Ag and 0.5Ag samples experience complete recrystallization, and their average grain sizes are 18.5 and 19.9 μm, respectively. Moreover, there are smaller grains distributed along the ED, which is common in extrusion bars due to the second phase inducing recrystallization nucleation and restricting grain growth [21]. Due to the synergistic effect of Gd/Y element and the extrusion process, the {0001} pole figures (PFs) and inverse pole figures (IPFs) referring to ED show more random grain orientations and weak texture characteristics.

Considering the texture difference, where the 0Ag sample shows a basal texture ($[10\bar{1}0]$//ED) and the 0.5Ag sample shows a C texture ([0001]// ED), Fig. 2 depicts the Schmid factor distribution of basal $\langle a \rangle$ slip, prismatic $\langle a \rangle$ slip, and pyramidal II $\langle c+a \rangle$ slip when loaded along the ED. Thus, the limited difference in initial textures can hardly influence the activation of multiple slip systems.

3.2 Uniaxial tensile properties at elevated temperature

Figure 3 shows the tensile stress–strain curves of the 0Ag and 0.5Ag extrusion bars under unidirectional tensile loading parallel to the ED at elevated temperatures. The 0.5Ag sample exhibits

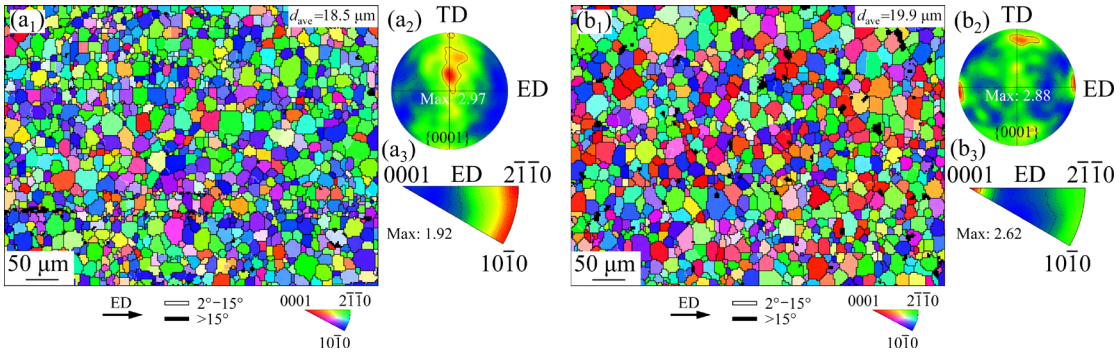

Fig. 1 Grain orientation distributions in 0Ag (a_1−a_3) and 0.5Ag (b_1−b_3) extrusion bars: (a_1, b_1) Orientation maps; (a_2, b_2) {0001} PFs; (a_3, b_3) IPFs referring to ED

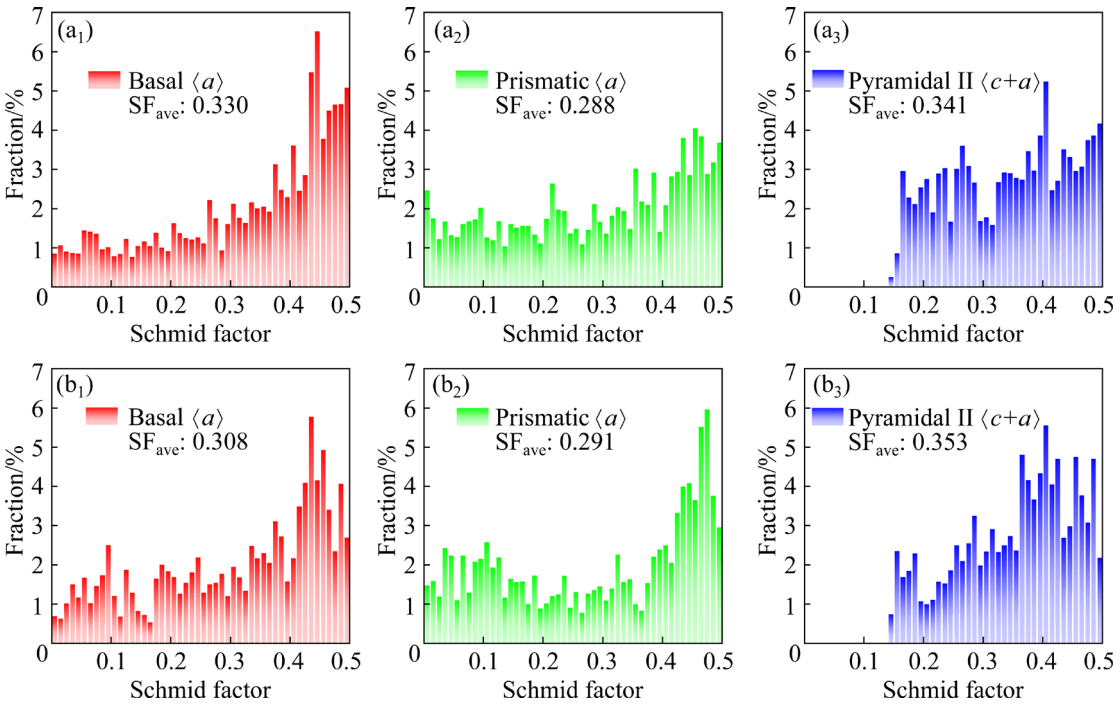

Fig. 2 Distribution of Schmid factors of basal ⟨a⟩ (a_1, b_1), prismatic ⟨a⟩ (a_2, b_2), and pyramidal II ⟨c+a⟩ (a_3, b_3) slip systems along ED: (a_1−a_3) 0Ag; (b_1−b_3) 0.5Ag

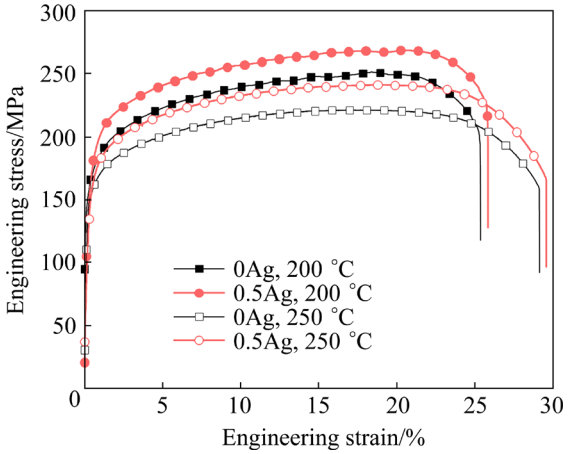

Fig. 3 Tensile stress–strain curves of 0Ag and 0.5Ag samples at 200 °C and 250 °C

higher strength than the 0Ag sample at the same temperature. At 200 °C, the UTS, TYS, and EL of the 0.5Ag sample are 267 MPa, 165 MPa, and 26.1%, respectively. When the temperature increases to 250 °C, the UTS and TYS decrease while the EL increases. On the one hand, the critical resolved shear stress (CRSS) of activating non-basal slip gradually decreases with the increase of deformation temperature [22,23]. Thus, the activation of multiple slip systems decreases the strength but improves the elongation of the 0Ag and 0.5Ag extrusion bars. On the other hand, compared to the Mg−Gd−Y−Zr alloys without Ag, due to differences in the atom size and electronegativity of

Mg, Gd, and Ag elements, more stable Gd/Ag co-segregation at grain boundaries can effectively restrict non-basal slip and improve the strength of Mg−Gd−Y−Zr−Ag alloys [24].

3.3 Tensile creep behaviors

Figure 4 shows the representative tensile creep curves of the extruded samples when subjected to tensile creep testing at 175−275 °C and 100 MPa for 100 h. By calculating the derivative of the creep strain with the corresponding creep time in the 0Ag and 0.5Ag samples, the steady creep rates at different temperatures are summarized in Table 1. At temperatures of 175−250 °C, the creep curves mainly exhibit a secondary creep stage. During this period, the creep rate remains constant and is maintained for a relatively long time. When the creep temperature increases to 275 °C, the 0.5Ag sample experiences a ternary stage followed by creep fracture for no more than 50 h. As given in Table 1, with increasing creep temperature, the steady creep rate gradually increases in extrusion bars with and without Ag. Moreover, the addition

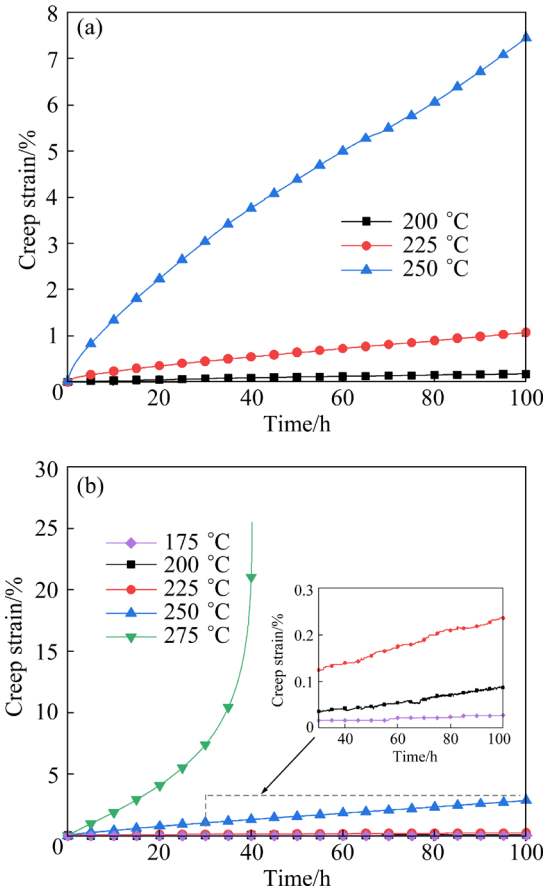

Fig. 4 Tensile creep curves of 0Ag and 0.5Ag samples crept at 100 MPa: (a) 0Ag; (b) 0.5Ag

Table 1 Steady creep rate of 0Ag and 0.5Ag samples crept at stress of 100 MPa

Sample	Temperature/°C	Steady creep rate/s^{-1}
0Ag	250	1.6×10^{-7}
	225	2.4×10^{-8}
	200	3.9×10^{-9}
0.5Ag	275	5.1×10^{-7}
	250	6.9×10^{-8}
	225	4.5×10^{-9}
	200	1.8×10^{-9}
	175	8.9×10^{-10}

of trace Ag leads to a lower steady creep rate of Mg−Gd−Y−Zr alloys. Thus, the samples containing Ag have a higher creep resistance.

Due to a near-constant creep rate in the secondary creep period, the relationship between the steady creep rate ($\dot{\varepsilon}$) and the applied stress (σ) of the extrusion bars can be plotted by the power law equation (Eq. (1)) [25]:

$$\dot{\varepsilon} = A\sigma^{n}\exp\left(\frac{-Q}{RT}\right) \tag{1}$$

where A is a constant related to the material components, R (8.314 J/(mol·K)) is the molar gas constant, n is the stress exponent, T is the thermodynamic temperature, and Q is the activation energy for creep. At similar creep parameters, the n values are about 3−7, and dislocation movement is the dominant creep mechanism in Mg−Gd series alloys [5,10,26]. Thus, this work focuses on evaluating creep mechanisms by the creep activation energy.

At a constant stress of 100 MPa, the creep activation energy Q can be described by Eq. (2):

$$Q = -R\frac{\partial \ln \dot{\varepsilon}}{\partial(1/T)} \tag{2}$$

According to the binary linear regression method based on Eq. (2), as shown in the fitting curves in Fig. 5, the creep activation energy of the 0Ag extrusion bar is about 155 kJ/mol, close to the self-diffusion energy of Mg (130−135 kJ/mol) [27]. Thus, the diffusion of Gd in Mg is the dominant creep mechanism in the 0Ag sample at 200−250 °C. Notably, the creep activation energies of the 0.5Ag sample are different in different temperature ranges. When creep temperatures are above 225 °C, the creep activation energy is about 208 kJ/mol, which

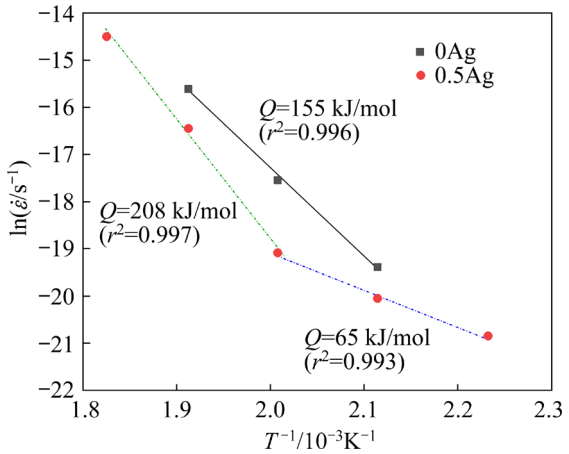

Fig. 5 Relationships between $\ln\dot{\varepsilon}$ and $1/T$ for 0Ag and 0.5Ag samples

is greater than the self-diffusion energy of Mg and close to the energy for activating the cross-slip of dislocations (229−325 kJ/mol) [27]; in contrast, when the temperature is below 225 °C, the activation energy is about 65 kJ/mol, which is lower than the energy for pipe diffusion in Mg (92 kJ/mol) and close to the energy for grain boundary diffusion (60−80 kJ/mol) [25]. The difference in the creep activation energy between the 0Ag and 0.5Ag samples further indicates that Ag addition improves the creep resistance at higher temperatures. Similar phenomena have been observed in other Mg−RE alloys, where the transition of creep activation energy is strongly related to the precipitation behavior, such as the formation of new phase or precipitate coarsening [10,28]. This indicates that the creep mechanism in the 0.5Ag extrusion bars shifts to dislocation creep from grain boundary diffusion with increasing creep temperature from 175 to 275 °C.

Figure 6 shows that dynamic precipitates, marked by green triangles, are enlarged in the 0.5Ag extrusion bar during the creep process. More importantly, abundant dislocations are marked in Fig. 6(c) by yellow arrows under the ***g***=[0002] vector, indicating that dislocations containing the ⟨*c*⟩ component are activated and the dislocation creep is the dominant creep mechanism.

3.4 Microstructure evolution after creep

Figure 7 shows the grain orientation and grain size of the 0Ag and 0.5Ag samples crept along the ED for 100 h at 250 °C. The average grain sizes of the 0Ag and 0.5Ag samples after creep are 18.8 and 20.0 μm, respectively. That is, grain growth does not occur during creep at 250 °C. In addition, due to the role of the tensile creep load, the grains rotate slightly to $[10\bar{1}0]$ //ED or $[2\bar{1}\bar{1}0]$ //ED orientations. However, as shown in Figs. 7(a_3, b_3), the whole texture intensity is weak in samples with and without Ag.

Figure 8 compares the microstructure characteristics of the 0Ag and 0.5Ag samples crept for 100 h at different temperatures. It is clearly observed that the grain boundaries appear as white lines in the BSE-SEM images, due to the accumulation of abundant Gd/Y/Ag particles. Moreover, with increasing the creep temperature, the width of precipitate free zones (PFZs) gradually increases. Specifically, PFZs are not obvious in the 0Ag and 0.5Ag samples crept at 200 °C. When the creep temperature increases to 250 °C, the width of PFZs in the 0.5Ag sample is 1.3 μm, which is less than that of the 0Ag sample. Moreover, under external stress, solute atoms and vacancies move in a particular direction during creep [5]. This is the

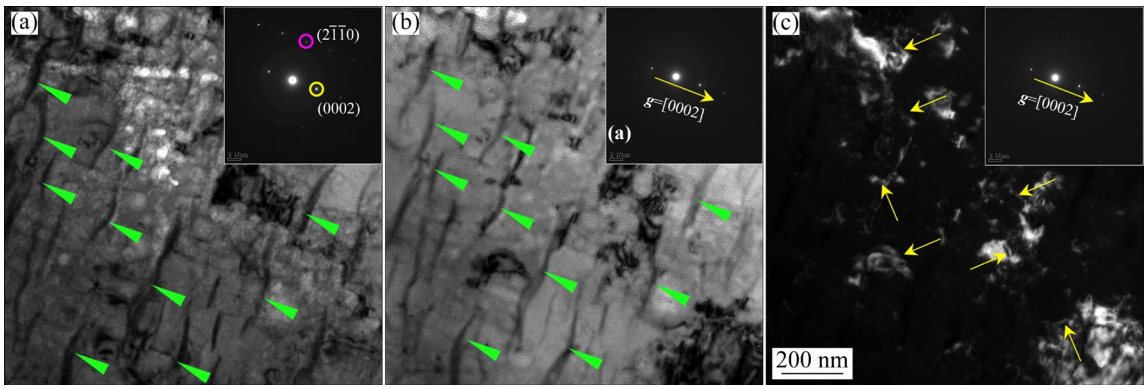

Fig. 6 TEM images of 0.5Ag sample crept at 250 °C: (a) Bright field image under ***B***=$[10\bar{1}0]$; (b) Bright field image under ***g***=[0002]; (c) Dark field image under ***g***=[0002]

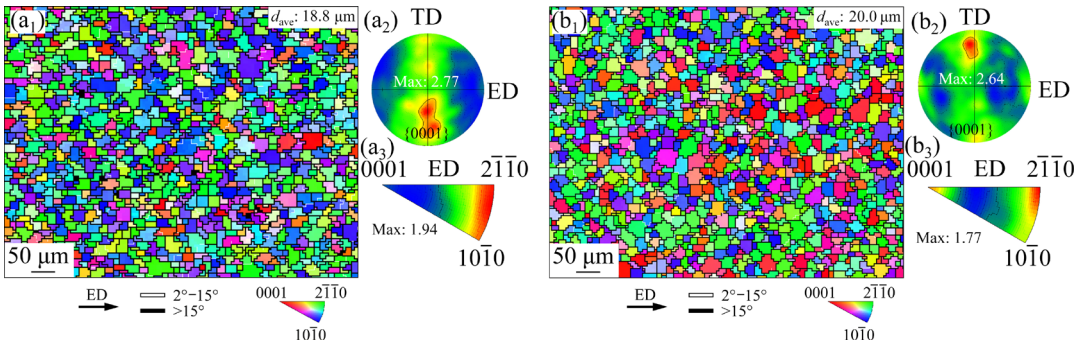

Fig. 7 Grain orientation distributions of 0Ag (a_1−a_3) and 0.5Ag (b_1−b_3) samples after creep at 250 °C for 100 h: (a_1, b_1) Orientation maps; (a_2, b_2) {0001} PFs; (a_3, b_3) IPFs referring to ED

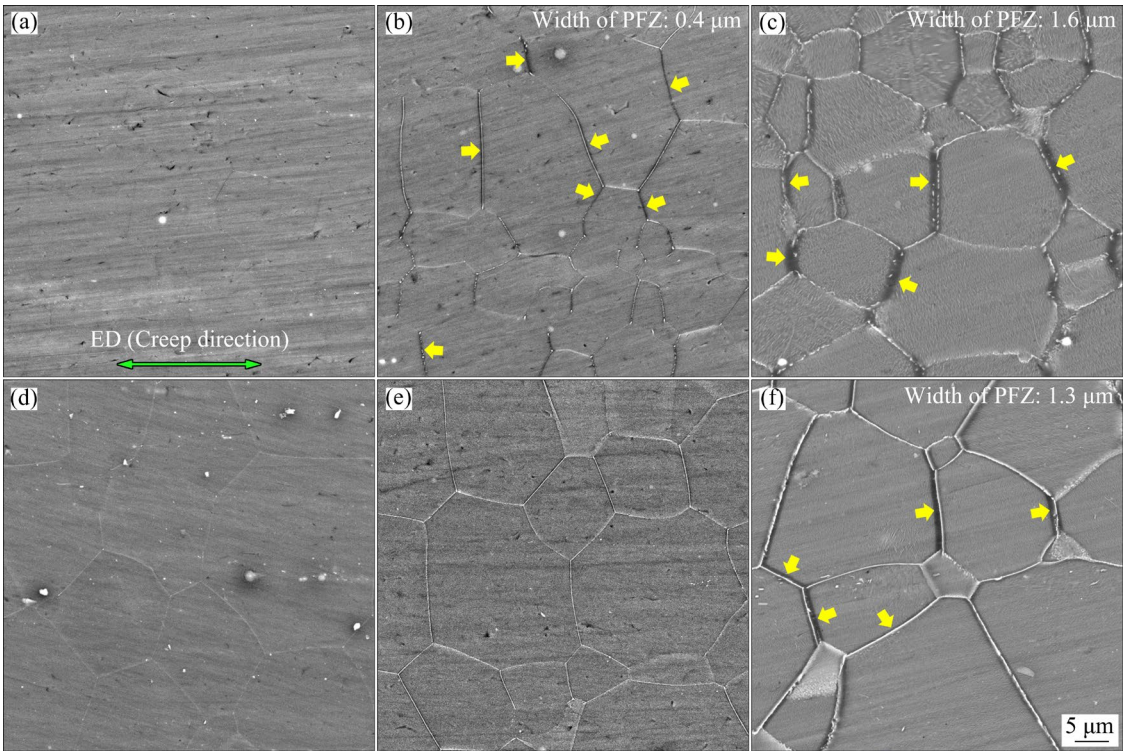

Fig. 8 BSE-SEM images of 0Ag (a−c) and 0.5Ag (d−f) extrusion bars crept at different temperatures for 100 h: (a, d) 200 °C; (b, e) 225 °C; (c, f) 250 °C (PFZs are marked by yellow arrows)

reason that these PFZs near grain boundaries are approximately perpendicular to the loading direction, meaning that these specially directional PFZs are predominantly induced by the exerted stress.

Due to their typical creep characteristics, such as precipitates and PFZs, the 0Ag and 0.5Ag samples crept at 250 °C are chosen to investigate the precipitate distribution in the grains and the elemental distribution adjacent to grain boundaries. Aided by HAADF−STEM technique, the β'-Mg_7RE precipitate morphology and distribution in the grain interior are shown in Fig. 9. Due to the tensile load in the creep process, these precipitates like chains are distributed in a special direction of [10$\bar{1}$0] (shown by the yellow dash lines) [29]. The volume fractions of the 0Ag and 0.5Ag samples crept for 100 h are 29.2% and 43.7%, respectively. This phenomenon is similar to the precipitation behavior of the peak-aged Mg−Gd−Y−Zr alloys, where adding Ag to Mg−Gd−Y−Zr alloys induces finer precipitates with a high density [4].

Figure 10 further shows the HAADF−STEM images with mapping near grain boundaries in the 0Ag and 0.5Ag samples crept at 250 °C. In the 0.5Ag sample, the grain boundaries are straight and

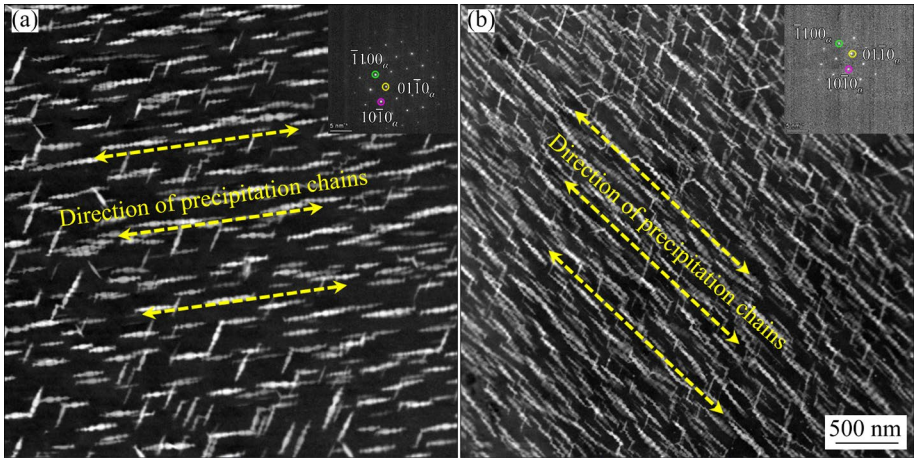

Fig. 9 HAADF−STEM images in grains of extrusion bars crept at 250 °C for 100 h: (a) 0Ag; (b) 0.5Ag

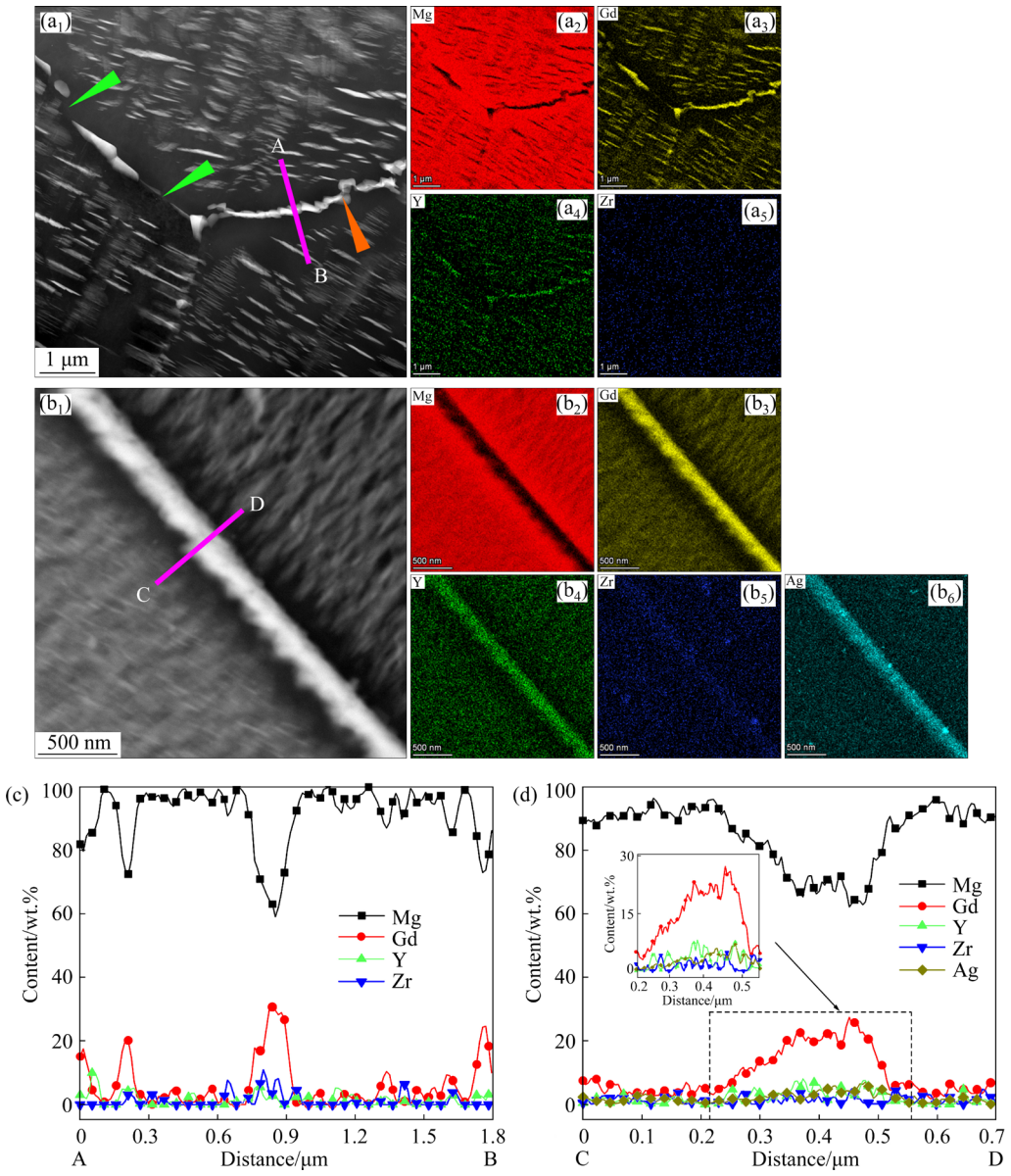

Fig. 10 HAADF−STEM images and EDS maps near grain boundary of extrusion bars of 0Ag (a_1−a_5) and 0.5Ag (b_1−b_6) samples crept at 250 °C for 100 h and element distributions along Line AB (c) in Fig. 10(a_1) and Line CD (d) in Fig. 10(b_1)

are attached to the second phase containing Gd, Y and Ag element. In contrast, the curved and cracked phase enriched in Gd and Y are distributed in grain boundaries of the 0Ag samples. Moreover, the second phase precipitated in grain boundaries after creep are identified as the β-Mg_5RE phase [30].

4 Discussion

Based on the foregoing calculation of Q values and previous investigations [10], the diffusion and dislocation creep are the main creep mechanisms when the 0Ag and 0.5Ag extrusion bars are crept at an applied stress of 100 MPa.

Effects of dynamic precipitates on creep resistance depend on their size and volume fraction. The refinement of precipitates contributes to improving the creep resistance [31]. Compared to that in the 0Ag samples, the dynamically precipitated β'-Mg_7RE phase stimulated by the Gd/Ag clusters is finer, with a higher density in the 0.5Ag samples. These β'-Mg_7RE precipitates can effectively pin dislocations, and with increasing density or decreasing size, their ability to restrict dislocation climb and glide increases. In addition, in the initial creep stage, Gd/Ag clusters may be easily formed and can pin dislocations [25]. Thus, when dislocation creep is the main creep mechanism, the 0.5Ag extrusion bars exhibit a lower steady creep rate and better creep resistance.

The creep resistance can also be affected by the precipitates located in the grain boundaries. With the increase in precipitates on the grain boundaries, vacancies inducing dislocation climb are suppressed, and dislocation accumulation occurs near precipitates, which enhances the creep resistance. Grain boundaries of the crept 0.5Ag sample are straight, and the β-Mg_5RE phases are distributed among them homogeneously and continuously. In contrast, the distribution of β-Mg_5RE phase is cracked (shown by the green triangles), and grain boundaries (shown by the orange triangles) collapse in the crept 0Ag sample, indicating that grain boundaries are not stable and grain boundary migration occurs. Thus, these continuous β-Mg_5RE phase along grain boundaries can effectively improve the stability of the grain boundaries, block mobile dislocations, and enhance the creep resistance. In addition, the segregation of Gd and Ag elements at grain boundaries can also restrict the movement of dislocations and grain boundaries, which leads to an improvement in the creep resistance.

Compared to the general grain boundary, PFZs are treated as blank regions with weak strength. Local stress concentrations can easily occur in PFZs and rapidly exceed the endurance of PFZs [10]. In Mg−Gd−Y-based alloys, different diffusion coefficients of solute atoms and Mg atoms lead to the development of PFZs under the applied stress. Combined with the results from ZHONG and ZHAO [32], the diffusion coefficients of Gd and Y in Mg are smaller than the Mg self-diffusion coefficient, while the diffusion coefficient of Ag in Mg is larger than the Mg self-diffusion coefficient. Furthermore, due to their atomic misfit and electronegativity, the extruded Mg−Gd−Y−Zr−Ag alloys exhibit Mg−Gd−Ag clusters or segregation with a stable low-energy condition [33]. Under these conditions, the PFZ width of the 0.5Ag samples is less than that of the 0Ag samples. Moreover, due to the lower volume fraction of β'-Mg_7RE precipitates and β-Mg_5RE phase in the 0Ag samples, dislocation movement is easier and the dislocation accumulation in grain boundaries can also cause the PDF widening [26]. Due to the synergistic role of solute atoms and dislocation migration, much narrower PFZs in the 0.5Ag samples lead to an improvement in the creep resistance.

Finally, adding Ag to Mg−Gd−Y−Zr alloys induces the formation of finer β'-Mg_7RE precipitates, more stable β-Mg_5RE phase on grain boundaries, and narrower PFZs, which leads to the suppression of dislocation movement and grain boundary migration, and improves the creep resistance of Mg−Gd−Y−Zr alloys.

5 Conclusions

(1) Grain growth does not occur during the creep process. However, due to the tensile creep load along the ED, the grains rotate slightly to the orientation of $[10\bar{1}0]$//ED or $[2\bar{1}\bar{1}0]$//ED.

(2) Under tensile creep loading along the ED, PFZs are formed near grain boundaries and perpendicular to the loading direction, while β'-Mg_7RE precipitates like chains are distributed in a special direction ($[10\bar{1}0]$).

(3) Adding Ag to Mg−Gd−Y−Zr alloys induces the formation of finer β'-Mg_7RE precipitates, more stable β-Mg_5RE phase at grain

boundaries, and narrower PFZs, which improves the creep resistance of Mg−Gd−Y−Zr alloys.

CRediT authorship contribution statement

Dong-dong ZHANG: Investigation, Data curation, Writing − Original draft; **Chu-ming LIU:** Project administration; **Ying-jie HUANG:** Data curation; **Yong-hao GAO:** Writing − Review & editing; **Shu-nong JIANG:** Supervision, Funding acquisition; **Ying-chun WAN:** Review, Supervision; **Zhi-yong CHEN:** Validation.

Declaration of competing interest

The authors declare that they have no known competing financial interests or personal relationships that could have appeared to influence the work reported in this paper.

Data Availability

The raw/processed data required to obtain these results cannot be shared at this moment since they are also part of an ongoing study.

Acknowledgments

This work was supported by the National Key R&D Program of China (No. 2021YFB3701100).

References

[1] XIE Dong-sheng, PAN Hu-cheng, PAN Zhen, ZHANG Dong-dong, TANG Wei-neng, YANG Chu-bin, XIE Hong-bo, REN Yu-ping, QIN Gao-wu. Achieving high heat-resistant property in dilute Mg−0.2Ce wrought alloy by retarding recrystallization process [J]. Journal of Alloys and Compounds, 2023, 958: 170410.

[2] WAN Ying-chun, TANG Bei, GAO Yong-hao, TANG Ling-ling, SHA Gang, ZHANG Bo, LIANG Ning-ning, LIU Chu-ming, JIANG Shu-nong, CHEN Zhi-yong, GUO Xue-yi, ZHAO Yong-hao. Bulk nanocrystalline high-strength magnesium alloys prepared via rotary swaging [J]. Acta Materialia, 2020, 200: 274−286.

[3] ZHANG Zi-jian, YUAN Lin, ZHENG Ming-yi, WEI Qing-he, SHAN De-bin, GUO Bin. Achievement of high strength and good ductility in the large-size AZ80 Mg alloy using a designed multi-directional forging process and aging treatment [J]. Journal of Materials Processing Technology, 2023, 311: 117828.

[4] ZHANG Dong-dong, LIU Chu-ming, JIANG Shu-nong, WAN Ying-chun, CHEN Zhi-yong. Effects of trace Ag on precipitation behavior and mechanical properties of extruded Mg−Gd−Y−Zr alloys [J]. Transactions of Nonferrous Metals Society of China, 2021, 31(11): 3394−3404.

[5] ZHANG Zhi-rou, HUO Qing-huan, LUO Lu, ZHANG Yu-xiu, XIAO Zhen-yu, LI Shi-qi, NAGAUMI H, YANG Xu-yue. Unexpected deterioration on the creep resistance of Mg−8wt.%Gd alloy via peak-aging treatment [J]. Materials Science and Engineering A, 2023, 869: 144809.

[6] XIAO Zhen-yu, XU Shi-wei, HUANG Wei-ying, LIU Hai-feng, YANG Xu-yue, XU Hai-kun, MA Chao, JIN Chen, LIN Zhan-hong. Unexpected effects on creep resistance of an extruded Mg−Bi alloy by Zn and Ca co-addition: experimental studies and first-principles calculations [J]. Journal of Materials Science and Technology, 2024, 201: 166−186. https:// doi.org/10.1016/j.jmst.2024.01.083

[7] ZHANG Yu-xiu, CHEN Dong-liang, NAGAUMI H, YANG Xu-yue. Highly improved creep resistance of hot-extruded Mg–0.9Mn–0.5Ce alloy by conventional forging [J]. Materials Science and Engineering A, 2022, 857: 144083.

[8] PATIL H, MARODKAR A, GHOSH A, BORKAR H. Effect of Ca addition on the microstructure and creep behaviour of AZ91 Mg alloy [J]. Materials Today: Proceedings, 2023, https://doi.org/10.1016/j.matpr.2023.03.056.

[9] GUAN Kai, ZHANG Jing-huai, YANG Qiang, LI Bai-shun, WU Rui-zhi, MENG Jian. Effects of trace Ca addition on microstructure and mechanical properties of as-cast Mg−Sm−Gd-based alloy [J]. Transactions of Nonferrous Metals Society of China, 2023, 33(1): 46−58.

[10] HUANG Ying-jie, LIU Chu-ming, WAN Ying-chun, JIANG Shu-nong, GAO Yong-hao, CHEN Zhi-yong. Effect of dislocation-induced aging precipitate bands on creep resistance of Mg−Gd−Y−Zr−Ag alloy [J]. Journal of Alloys and Compounds, 2023, 960: 170633.

[11] XU Chao, NAKATA T, FAN Guo-hua, LI Xue-wen, TANG Guang-ze, KAMADO S. Enhancing strength and creep resistance of Mg−Gd−Y−Zn−Zr alloy by substituting Mn for Zr [J]. Journal of Magnesium and Alloys, 2019, 7(3): 388−399.

[12] ZHOU Xiao-jie, YAO Yuan, ZHANG Jian, Chen Xiao-min, HUANG Wei-ying, PAN Jing, WANG Hao-ran, WENG Mao-peng. A high-performance Mg−4.9Gd−3.2Y−1.1Zn−0.5Zr alloy via multidirectional forging after analyzing its compression behavior [J]. Journal of Materials Science and Technology, 2021, 70: 156−167.

[13] ZHANG Zhi-rou, HUO Qing-huan, ZHANG Yu-xiu, HE Yang, NAGAUMI H, YANG Xu-yue. Unraveling the individual effect of yttrium and neodymium on the precipitate-free zone development and the dislocation creep mechanism of Mg−Y−Nd alloy [J]. Materials Characterization, 2023, 195: 112537.

[14] MEIER J M, CARIS J, LUO A A. Towards high strength cast Mg–RE based alloys: Phase diagrams and strengthening mechanisms [J]. Journal of Magnesium and Alloys, 2022, 10(6): 1401−1427.

[15] CHEN Xiao-ya, LI Quan-an, YAN Jing-long, CHEN Pei-jun. Microstructure and high temperature mechanical properties of the Mg−Gd−Y(−Nd)−Zr alloy [J]. Journal of Materials Research and Technology, 2023, 24: 866−878.

[16] MOVAHEDI-RAD A, MAHMUDI R, WU Guo-hua, NODOOSHAN H R J. Enhanced superplasticity in an extruded high strength Mg−Gd−Y−Zr alloy with Ag addition [J]. Journal of Alloys and Compounds, 2015, 626: 309−313.

[17] NAJAFI S, MAHMUDI R. Enhanced microstructural stability and mechanical properties of the Ag-containing Mg−Gd−Y alloys [J]. Journal of Magnesium and Alloys, 2020, 8(4): 1109−1119.

[18] HUANG Cen, LIU Chu-ming, JIANG Shu-nong, WAN Ying-chun. Enhanced age-hardening response and

mechanical properties of the Mg−Gd−Y−Zn−Zr alloy by trace Ag addition [J]. Journal of Alloys and Compounds, 2021, 874: 159825.
[19] ZHANG Dong-dong, LIU Chu-ming, JIANG Shu-nong, GAO Yong-hao, WAN Ying-chun, CHEN Zhi-yong. Effects of dynamic recrystallization mechanisms on texture evolution in Mg−Gd−Y−Zr−Ag alloy during hot compression [J]. Journal of Alloys and Compounds, 2023, 944: 169190.
[20] ZHANG Dong-dong, LIU Chu-ming, JIANG Shu-nong, GAO Yong-hao, WAN Ying-chun, CHEN Zhi-yong. Effects of extrusion process on microstructure, precipitates and mechanical properties of Mg−Gd−Y−Zr−Ag alloys [J]. Materials Science and Engineering A, 2022, 856: 143990.
[21] ZHANG Dong-dong, LIU Chu-ming, JIANG Shu-nong, GAO Yong-hao, WAN Ying-chun, CHEN Zhi-yong, ZHANG Zong-liang. Formation of fine-grain rings on the surface region of the extruded Mg−Gd−Y−Zr−Ag rod [J]. Advanced Engineering Materials, 2023, 25: 2201802.
[22] NIE J F, SHIN K S, ZENG Zhuo-ran. Microstructure, deformation, and property of wrought magnesium alloys [J]. Metallurgical and Metallurgical and Materials: A, 2020, 51(12): 6045−6109.
[23] FAN Hai-dong, WANG Qing-yuan, TIAN Xiao-bao, EI-AWADY J A. Temperature effects on the mobility of pyramidal ⟨*c*+*a*⟩ dislocations in magnesium [J]. Scripta Materialia, 2017, 127: 68−71.
[24] WU Zhao-xuan, AHMAD R, YIN Bing-lun, SANDLOBES S, CURTIN W A. Mechanistic origin and prediction of enhanced ductility in magnesium alloys [J]. Science, 2018, 359(6374): 447−452.
[25] DONG Xi-xi, FENG Ling-yun, WANG Shi-hao, JI Gang, ADDAD A, YANG Hai-lin, NYBERG E A, JI Shou-xun. On the exceptional creep resistance in a die-cast Gd-containing Mg alloy with Al addition [J]. Acta Materialia, 2022, 232: 117957.
[26] QIN He, YANG Guang-yu, KAN Zhi-yong, WANG Chun-hui, OUYANG Shu-xia, JIE Wan-qi. Effect of substituting Gd with 3 wt.% Nd on high temperature creep behaviors of peak-aged Mg−10Gd−0.4Zr casting Mg alloy [J]. Journal of Materials Research and Technology, 2023, 25: 5781−5794.
[27] ZHANG Dong-dong, YANG Shuo, MENG Fan-zhi, TIAN Zheng, XU Hong, CAO Zhan-yi, MENG Jian. Compressive creep behavior of extruded Mg−4Sm−2Yb−0.6Zn−0.4Zr alloy [J]. Materials Science and Engineering A, 2021, 809: 140929.
[28] WANG Huan, WANG Qu-dong, BOEHLERT C J, YIN Dong-di, YUAN J. Tensile and compressive creep behavior of extruded Mg−10Gd−3Y−0.5Zr (wt.%) alloy [J]. Materials Characterization, 2015, 99: 25−37.
[29] SHEN Si-min, ZHUANG Yong-peng, LI Ming, WANG Hong-xia, WANG Li-fei, CHENG Wei-li, LI Hang, HOU Hua, SHIN K S. Effects of stress loading mode on microstructures and properties of Mg−9Gd−2Nd−0.5Zr alloy treated by creep aging [J]. Journal of Magnesium and Alloys, 2023, 11(11): 4263−4273.
[30] SHI Hui, HUANG Yuan-ding, YANG Li-xiang, LIU Chun-quan, DIERINGA H, LU Chong, Xiao Lv, WILLUMEIT R, HORT N. Compressive creep behavior and microstructural evolution of sand-cast and peak-aged Mg−12Gd−0.4Zr alloy at 250 °C [J]. Materials Science and Engineering A, 2023, 882: 145422.
[31] ALI M A, LÓPEZ-GALILEA I, GAO Si-wen, RUTTERT B, AMIN W, SHCHYGLO O, HARTMAIER A, THEISEN W, STEINBACH I. Effect of γ' precipitate size on hardness and creep properties of Ni-base single crystal superalloys: Experiment and simulation [J]. Materialia, 2020, 12(8): 100692.
[32] ZHONG Wei, ZHAO Ji-cheng. A comprehensive diffusion mobility database comprising 23 elements for magnesium alloys [J]. Acta Materialia, 2020, 201: 191−208.
[33] ZHANG Dong-dong, LIU Chu-ming, JIANG Shu-nong, GAO Yong-hao, WAN Ying-chun, CHEN Zhi-yong. Effects of trace Ag on the dynamic recrystallization and mechanical properties of Mg−Gd−Y−Zr alloy [J]. Materials Science and Engineering A, 2023, 880: 145377.

Ag 微合金化对 Mg−Gd−Y−Zr 挤压棒高温蠕变性能的影响

张冬冬[1]，刘楚明[2]，黄英杰[1]，高永浩[1]，蒋树农[1]，万迎春[3]，陈志永[1]

1. 中南大学 材料科学与工程学院，长沙 410083；
2. 湖南镁宇科技有限公司，岳阳 414000；
3. 中南大学 轻合金研究院，长沙 410083

摘　要：通过拉伸试验和蠕变试验，并借助于电子背散射衍射和透射电子显微术，系统研究了微量 Ag 元素对 Mg−7.5Gd−1.5Y−0.4Zr (质量分数，%)挤压棒在 175~275 °C 的拉伸强度和抗蠕变性能的影响。结果表明，添加微量 Ag 元素可提高 Mg−Gd−Y−Zr 合金的高温拉伸强度和抗蠕变性能。蠕变过程中，合金在晶界附近形成垂直于加载方向的无沉淀析出带(PFZs)，晶内形成沿 $[10\bar{1}0]$ 取向呈链状分布的 β'-Mg_7RE 相。添加 Ag 元素后，PFZs 更窄，晶内 β'-Mg_7RE 相尺寸更细，晶界 β-Mg_5RE 相结构更加稳定，因此，位错运动受抑制，合金抗蠕变性能更好。

关键词：微量 Ag；抗蠕变性能；无沉淀析出带；挤压；Mg−Gd−Y−Zr 合金

(Edited by Bing YANG)